PROCEEDINGS OF THE ROYAL SOCIETY A

Proc. R. Soc. A (2008) **464**, 1525–1541
doi:10.1098/rspa.2007.0209
Published online 4 March 2008

Interacting dipole pairs on a rotating sphere

By Paul K. Newton[1,2,*] and Houman Shokraneh[1,2]

[1]*Department of Aerospace and Mechanical Engineering, and*
[2]*Department of Mathematics, University of Southern California, Los Angeles, CA 90089-1191, USA*

The evolution, interaction and scattering of $2N$ point vortices grouped into equal and opposite pairs (N-dipoles) on a rotating unit sphere are studied. A new coordinate system made up of centres of vorticity and centroids associated with each dipole is introduced. With these coordinates, the nonlinear equations for an isolated dipole diagonalize and one directly obtains the equation for geodesic motion on the sphere for the dipole centroid. When two or more dipoles interact, the equations are viewed as an interacting billiard system on the sphere — charged billiards — with long-range interactions causing the centroid trajectories to deviate from their geodesic paths. Canonical interactions are studied both with and without rotation. For two dipoles, the four basic interactions are described as *exchange-scattering*, *non-exchange-scattering*, *loop-scattering* (head on) and loop-scattering (chasing) interactions. For three or more dipoles, one obtains a richer variety of interactions, although the interactions identified in the two-dipole case remain fundamental.

Keywords: *N*-vortex problem; dipole scattering; charged billiard system

1. Introduction

Vortex dipoles play an important role in the transport and mixing of particles (both passive and active) in oceanographic and atmospheric flows, yet rarely do they appear in complete isolation. Typically, they are forced to interact with a background field, such as jet stream, ocean currents or other multipoles. See McDonald (1999) for a general discussion of geophysical vortices and the main important physical mechanisms, and DiBattista & Polvani (1998) for a more focused study of a single dipole interacting with a background vorticity field. Despite this fact, a study of their interactions on the rotating sphere has not been carried out. In the unbounded plane, a pioneering study of the scattering process between dipoles is described by Eckhardt & Aref (1988). Unlike the unbounded plane, since the sphere is compact, the dipoles cannot escape to infinity and the dynamics typically involves multiple 'scattering events' and orbits that are closed or at least densely covering the accessible portion of the sphere over long times. This means that for almost all initial conditions, a scattering event or multiple scattering events will ultimately take place and play an important role in the subsequent dynamics. In statistical studies of multi-vortex populations,

* Author and address for correspondence: Department of Aerospace and Mechanical Engineering, University of Southern California, Los Angeles, CA 90089-1191, USA (newton@usc.edu).

Received 7 September 2007
Accepted 6 February 2008

such as that carried out by Dritschel & Zabusky (1996), these scattering events can play a significant role in the interpretation of complex spectral signatures and equilibrium and non-equilibrium kinetic theories based on point vortices, such as those in Marmanis (1998), Newton & Mezić (2002), Chavanis (2007) and Chavanis & Lemou (2007), must ultimately account for them.

When there is only one dipole on the non-rotating sphere (or on any surface of constant curvature) it moves periodically along a closed geodesic as shown in Kimura (1999), allowing the assignment of a 'natural' frequency, ω. However, when two or more dipoles interact, or when the sphere rotates, the dipole trajectories are more complex. For these cases, it is useful to introduce coordinates that capture both the geodesic flow and the interactions. We introduce such a 'dipole coordinate system' in this paper. For a general background on the dynamical system we consider, in particular, the limitations and consequences of our one-way coupled treatment of rotation, see Jamaloodeen & Newton (2006), Newton & Shokraneh (2006), and Newton & Sakajo (2007). In §2, we describe the dipole coordinate system that we use to analyse the scattering of multiple dipoles. In §3, we focus on the most important case of two interacting dipoles and identify the main scattering modes, which we call *exchange scattering*, *non-exchange scattering* and *loop scattering*. When three or more dipoles interact (as described in §4), since typically only two of the three interact at one time, these same modes frequently appear. Occasionally, however, with three or more dipoles, the initial conditions are just right so that a collision occurs involving more than two dipoles. We show some examples of this non-generic situation as well. Of course, generically we know that when three or fewer point vortices interact on the sphere, the trajectories are either periodic or quasi-periodic (Kidambi & Newton 1998; Newton 2001), whereas when four or more point vortices interact, the trajectories are chaotic (Newton & Ross 2006). We start by writing the system of $2N$ point vortices on the one-way coupled rotating sphere (see Newton & Shokraneh 2006), preparing to group them into a system of N-dipoles:

$$\dot{\boldsymbol{x}}_\alpha = \frac{1}{4\pi} {\sum_{\beta=1}^{2N}}' \Gamma_\beta \frac{\boldsymbol{x}_\beta \times \boldsymbol{x}_\alpha}{(1-\boldsymbol{x}_\alpha \cdot \boldsymbol{x}_\beta)} + \Omega \hat{\boldsymbol{e}}_z \times \boldsymbol{x}_\alpha \quad (\alpha = 1, \ldots, 2N), \tag{1.1}$$

where

$$\boldsymbol{x}_\alpha \in \mathbb{R}^3, \qquad ||\boldsymbol{x}_\alpha|| = 1$$

and

$$\boldsymbol{\Gamma} = (\Gamma_1, \ldots, \Gamma_N; \ -\Gamma_1, \ldots, -\Gamma_N) \in \mathbb{R}^{2N}.$$

With this notation, the two point vortices located at $(\boldsymbol{x}_\alpha, \boldsymbol{x}_{\alpha+N})$ form a dipole pair, for each $\alpha = 1, \ldots, N$ of the N dipoles. The prime on the summation in equation (1.1) states that the singular term $\beta = \alpha$ is omitted and initially the vortices are located at the given positions $\boldsymbol{x}_\alpha(0) \in \mathbb{R}^3$, $(\alpha = 1, \ldots, 2N)$. It is advantageous to split the system into a pair of equations for each of the N dipoles, hence

$$\dot{\boldsymbol{x}}_\alpha = \frac{1}{4\pi} {\sum_{\beta=1}^{N}}' \Gamma_\beta \left[\frac{\boldsymbol{x}_\beta \times \boldsymbol{x}_\alpha}{(1-\boldsymbol{x}_\alpha \cdot \boldsymbol{x}_\beta)} - \frac{\boldsymbol{x}_{\beta+N} \times \boldsymbol{x}_\alpha}{(1-\boldsymbol{x}_\alpha \cdot \boldsymbol{x}_{\beta+N})} \right] - \frac{\Gamma_\alpha}{4\pi} \frac{\boldsymbol{x}_{\alpha+N} \times \boldsymbol{x}_\alpha}{(1-\boldsymbol{x}_\alpha \cdot \boldsymbol{x}_{\alpha+N})}$$

$$+ \Omega \hat{\boldsymbol{e}}_z \times \boldsymbol{x}_\alpha, \tag{1.2}$$

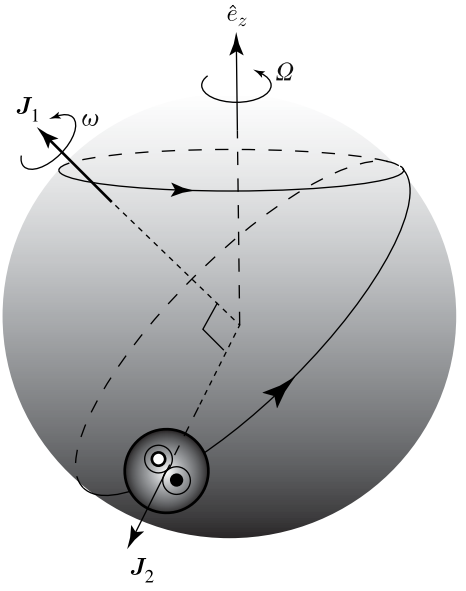

Figure 1. Dipole coordinates on a rotating sphere for a single dipole. $\boldsymbol{J}_1$ is the centre-of-vorticity vector, which cuts a spherical cap perpendicular to the axis of rotation, and $\boldsymbol{J}_2$ ($\perp$ to $\boldsymbol{J}_1$) is the centroid of the dipole, which traces a geodesic on the sphere in the absence of rotation. The overall motion is a superposition of rotations about two axes, with two independent frequencies ω, Ω.

$$\dot{\boldsymbol{x}}_{\alpha+N} = \frac{1}{4\pi}\sum_{\beta=1}^{N}{}' \Gamma_\beta \left[\frac{\boldsymbol{x}_\beta \times \boldsymbol{x}_{\alpha+N}}{(1-\boldsymbol{x}_{\alpha+N}\cdot\boldsymbol{x}_\beta)} - \frac{\boldsymbol{x}_{\beta+N}\times\boldsymbol{x}_{\alpha+N}}{(1-\boldsymbol{x}_{\alpha+N}\cdot\boldsymbol{x}_{\beta+N})}\right] - \frac{\Gamma_\alpha}{4\pi}\frac{\boldsymbol{x}_{\alpha+N}\times\boldsymbol{x}_\alpha}{(1-\boldsymbol{x}_\alpha\cdot\boldsymbol{x}_{\alpha+N})} + \Omega\hat{\boldsymbol{e}}_z\times\boldsymbol{x}_{\alpha+N}, \tag{1.3}$$

where $\alpha=1, \ldots, N$. The coordinates of the two point vortices constituting a dipole are then $(\boldsymbol{x}_\alpha, \boldsymbol{x}_{\alpha+N})$, and Ω is the rotational frequency of the sphere about the North Pole axis.

2. Dipole coordinates

(*a*) *Coordinate transformation*

The new set of dipole-based coordinates $(\boldsymbol{J}_\alpha, \boldsymbol{J}_{\alpha+N})$ are derived from the original vortex coordinates $(\boldsymbol{x}_\alpha, \boldsymbol{x}_{\alpha+N})$ via the linear transformation

$$\boldsymbol{J}_\alpha \equiv \Gamma_\alpha(\boldsymbol{x}_\alpha - \boldsymbol{x}_{\alpha+N}), \tag{2.1}$$

$$\boldsymbol{J}_{\alpha+N} \equiv \Gamma_\alpha(\boldsymbol{x}_\alpha + \boldsymbol{x}_{\alpha+N}). \tag{2.2}$$

The vectors $\boldsymbol{J}_\alpha$ represent the centres of vorticity of each of the N dipoles, while $\boldsymbol{J}_{\alpha+N}$ are their centroids, as shown in figure 1 for the simplest case $N=1$. The

inverse transformation is given by

$$\boldsymbol{x}_\alpha = \frac{1}{2\Gamma_\alpha}(\boldsymbol{J}_\alpha + \boldsymbol{J}_{\alpha+N}), \tag{2.3}$$

$$\boldsymbol{x}_{\alpha+N} = -\frac{1}{2\Gamma_\alpha}(\boldsymbol{J}_\alpha - \boldsymbol{J}_{\alpha+N}). \tag{2.4}$$

In matrix form, the transformation is

$$\hat{\mathbb{J}} = \mathbb{M}\hat{\boldsymbol{x}}, \tag{2.5}$$

where

$$\hat{\mathbb{J}} \equiv \begin{pmatrix} \boldsymbol{J}_1 \\ \vdots \\ \boldsymbol{J}_N \\ \boldsymbol{J}_{N+1} \\ \vdots \\ \boldsymbol{J}_{2N} \end{pmatrix}, \qquad \hat{\boldsymbol{x}} \equiv \begin{pmatrix} \boldsymbol{x}_1 \\ \vdots \\ \boldsymbol{x}_N \\ \boldsymbol{x}_{N+1} \\ \vdots \\ \boldsymbol{x}_{2N} \end{pmatrix} \tag{2.6}$$

and $\mathbb{M}$ is a $2N\times 2N$ matrix with block structure:

$$\mathbb{M} \equiv \begin{pmatrix} \boldsymbol{M}_\Gamma & -\boldsymbol{M}_\Gamma \\ \boldsymbol{M}_\Gamma & \boldsymbol{M}_\Gamma \end{pmatrix}. \tag{2.7}$$

$\boldsymbol{M}_\Gamma \in \mathbb{R}^N \times \mathbb{R}^N$ is the diagonal matrix given by

$$\boldsymbol{M}_\Gamma = \begin{pmatrix} \Gamma_1 & \dots & 0 \\ \vdots & \vdots & \vdots \\ 0 & \dots & \Gamma_N \end{pmatrix}. \tag{2.8}$$

In these coordinates, we have the following.

Theorem 2.1. *Let the centre-of-vorticity vector associated with equation (1.1) be defined as* $\boldsymbol{J} = (J_x, J_y, J_z) = \sum_{\alpha=1}^{N} \boldsymbol{J}_\alpha$. *Then (i)* $\|\boldsymbol{J}\| = \text{const.}$, $J_x^2 + J_y^2 = C_1$, $J_z = C_2$ *and (ii)* $\boldsymbol{J}_\alpha \perp \boldsymbol{J}_{\alpha+N}$.

Proof. The first part of the proposition in proven in Newton & Shokraneh (2006) and is not repeated here. To see that $\boldsymbol{J}_\alpha \perp \boldsymbol{J}_{\alpha+N}$, consider

$$\begin{aligned} \boldsymbol{J}_\alpha \cdot \boldsymbol{J}_{\alpha+N} &\equiv \Gamma_\alpha^2(\boldsymbol{x}_\alpha - \boldsymbol{x}_{\alpha+N})\cdot(\boldsymbol{x}_\alpha + \boldsymbol{x}_{\alpha+N}), \\ &= \Gamma_\alpha^2(\boldsymbol{x}_\alpha \cdot \boldsymbol{x}_\alpha + \boldsymbol{x}_\alpha \cdot \boldsymbol{x}_{\alpha+N} - \boldsymbol{x}_{\alpha+N}\cdot \boldsymbol{x}_\alpha - \boldsymbol{x}_{\alpha+N}\cdot \boldsymbol{x}_{\alpha+N}), \end{aligned} \tag{2.9}$$

$$\boldsymbol{J}_\alpha \cdot \boldsymbol{J}_{\alpha+N} = (\|\boldsymbol{x}_\alpha\|^2 - \|\boldsymbol{x}_{\alpha+N}\|^2) = 0. \tag{2.10}$$

■

To obtain the evolution equations in the dipole coordinates, we differentiate equations (2.3) and (2.4),

$$\dot{\boldsymbol{J}}_\alpha + \dot{\boldsymbol{J}}_{\alpha+N} = \frac{\Gamma_\alpha}{2\pi} {\sum_{\beta=1}^{N}}' \Gamma_\beta \left[\frac{\boldsymbol{x}_\beta \times \boldsymbol{x}_\alpha}{(1-\boldsymbol{x}_\alpha \cdot \boldsymbol{x}_\beta)} - \frac{\boldsymbol{x}_{\beta+N} \times \boldsymbol{x}_\alpha}{(1-\boldsymbol{x}_\alpha \cdot \boldsymbol{x}_{\beta+N})} \right]$$

$$- \frac{\Gamma_\alpha^2}{2\pi} \frac{\boldsymbol{x}_{\alpha+N} \times \boldsymbol{x}_\alpha}{(1-\boldsymbol{x}_\alpha \cdot \boldsymbol{x}_{\alpha+N})} + 2\Gamma_\alpha \Omega \hat{\boldsymbol{e}}_z \times \boldsymbol{x}_\alpha, \tag{2.11}$$

$$\dot{\boldsymbol{J}}_\alpha - \dot{\boldsymbol{J}}_{\alpha+N} = -\frac{\Gamma_\alpha}{2\pi} {\sum_{\beta=1}^{N}}' \Gamma_\beta \left[\frac{\boldsymbol{x}_\beta \times \boldsymbol{x}_{\alpha+N}}{(1-\boldsymbol{x}_{\alpha+N} \cdot \boldsymbol{x}_\beta)} - \frac{\boldsymbol{x}_{\beta+N} \times \boldsymbol{x}_{\alpha+N}}{(1-\boldsymbol{x}_{\alpha+N} \cdot \boldsymbol{x}_{\beta+N})} \right]$$

$$+ \frac{\Gamma_\alpha^2}{2\pi} \frac{\boldsymbol{x}_{\alpha+N} \times \boldsymbol{x}_\alpha}{(1-\boldsymbol{x}_\alpha \cdot \boldsymbol{x}_{\alpha+N})} - 2\Gamma_\alpha \Omega \hat{\boldsymbol{e}}_z \times \boldsymbol{x}_{\alpha+N}. \tag{2.12}$$

Then, using the fact that

$$\boldsymbol{x}_\alpha \times \boldsymbol{x}_{\alpha+N} = \frac{1}{2\Gamma_\alpha^2} \boldsymbol{J}_\alpha \times \boldsymbol{J}_{\alpha+N}, \tag{2.13}$$

$$\boldsymbol{x}_\alpha \cdot \boldsymbol{x}_{\alpha+N} = -\frac{1}{4\Gamma_\alpha^2} (\|\boldsymbol{J}_\alpha\|^2 - \|\boldsymbol{J}_{\alpha+N}\|^2), \tag{2.14}$$

we can add and subtract the two equations to obtain

$$\dot{\boldsymbol{J}}_\alpha = \Omega \hat{e}_z \times \boldsymbol{J}_\alpha + \frac{\Gamma_\alpha}{4\pi} {\sum_{\beta=1}^{N}}' \Gamma_\beta \left\{ \frac{(\boldsymbol{J}_\beta + \boldsymbol{J}_{\beta+N}) \times (\boldsymbol{J}_\alpha + \boldsymbol{J}_{\alpha+N})}{4\Gamma_\alpha \Gamma_\beta - (\boldsymbol{J}_\alpha + \boldsymbol{J}_{\alpha+N}) \cdot (\boldsymbol{J}_\beta + \boldsymbol{J}_{\beta+N})} \right.$$

$$- \frac{(\boldsymbol{J}_\beta - \boldsymbol{J}_{\beta+N}) \times (\boldsymbol{J}_\alpha + \boldsymbol{J}_{\alpha+N})}{4\Gamma_\alpha \Gamma_\beta + (\boldsymbol{J}_\alpha + \boldsymbol{J}_{\alpha+N}) \cdot (\boldsymbol{J}_\beta - \boldsymbol{J}_{\beta+N})} + \frac{(\boldsymbol{J}_\beta + \boldsymbol{J}_{\beta+N}) \times (\boldsymbol{J}_\alpha - \boldsymbol{J}_{\alpha+N})}{4\Gamma_\alpha \Gamma_\beta + (\boldsymbol{J}_\alpha - \boldsymbol{J}_{\alpha+N}) \cdot (\boldsymbol{J}_\beta + \boldsymbol{J}_{\beta+N})}$$

$$\left. + \frac{(\boldsymbol{J}_\beta - \boldsymbol{J}_{\beta+N}) \times (\boldsymbol{J}_\alpha - \boldsymbol{J}_{\alpha+N})}{4\Gamma_\alpha \Gamma_\beta - (\boldsymbol{J}_\alpha - \boldsymbol{J}_{\alpha+N}) \cdot (\boldsymbol{J}_\beta - \boldsymbol{J}_{\beta+N})} \right\}, \tag{2.15}$$

$$\dot{\boldsymbol{J}}_{\alpha+N} = \frac{1}{4\pi} \frac{\boldsymbol{J}_\alpha \times \boldsymbol{J}_{\alpha+N}}{1 + \frac{1}{4\Gamma_\alpha^2} (\|\boldsymbol{J}_\alpha\|^2 - \|\boldsymbol{J}_{\alpha+N}\|^2)} + \Omega \hat{e}_z \times \boldsymbol{J}_{\alpha+N}$$

$$+ \frac{\Gamma_\alpha}{4\pi} {\sum_{\beta=1}^{N}}' \Gamma_\beta \left\{ \frac{(\boldsymbol{J}_\beta + \boldsymbol{J}_{\beta+N}) \times (\boldsymbol{J}_\alpha + \boldsymbol{J}_{\alpha+N})}{4\Gamma_\alpha \Gamma_\beta - (\boldsymbol{J}_\alpha + \boldsymbol{J}_{\alpha+N}) \cdot (\boldsymbol{J}_\beta + \boldsymbol{J}_{\beta+N})} \right.$$

$$- \frac{(\boldsymbol{J}_\beta - \boldsymbol{J}_{\beta+N}) \times (\boldsymbol{J}_\alpha + \boldsymbol{J}_{\alpha+N})}{4\Gamma_\alpha \Gamma_\beta + (\boldsymbol{J}_\alpha + \boldsymbol{J}_{\alpha+N}) \cdot (\boldsymbol{J}_\beta + \boldsymbol{J}_{\beta+N})} - \frac{(\boldsymbol{J}_\beta - \boldsymbol{J}_{\beta+N}) \times (\boldsymbol{J}_\alpha - \boldsymbol{J}_{\alpha+N})}{4\Gamma_\alpha \Gamma_\beta - (\boldsymbol{J}_\alpha - \boldsymbol{J}_{\alpha+N}) \cdot (\boldsymbol{J}_\beta - \boldsymbol{J}_{\beta+N})}$$

$$\left. - \frac{(\boldsymbol{J}_\beta - \boldsymbol{J}_{\beta+N}) \times (\boldsymbol{J}_\alpha - \boldsymbol{J}_{\alpha+N})}{4\Gamma_\alpha \Gamma_\beta - (\boldsymbol{J}_\alpha - \boldsymbol{J}_{\alpha+N}) \cdot (\boldsymbol{J}_\beta - \boldsymbol{J}_{\beta+N})} \right\}. \tag{2.16}$$

Equations (2.15) and (2.16) are the full set of equations ($\alpha = 1, \ldots, N$) we use for the system of N-interacting dipoles. To clarify why these new coordinates are so useful, we first consider the case of an isolated dipole ($N=1$) as shown in figure 1.

(*b*) *N*=1*: geodesic motion*

The advantage of using these coordinates can be seen by noting that the summation terms in (2.15) and (2.16) account for the dipole interactions, while the preceding terms account for the natural tendency for each dipole to follow a geodesic (Kimura 1999). This is brought out in theorem 2.2.

Theorem 2.2.

(*i*) *For* $N=1$ *and* $\Omega=0$, *the equations* (*2.15*) *and* (*2.16*) *decouple*

$$\dot{\boldsymbol{J}}_1 = 0, \tag{2.17}$$

$$\dot{\boldsymbol{J}}_2 = \frac{1}{4\pi}\frac{\boldsymbol{J}_1\times\boldsymbol{J}_2}{1+(\|\boldsymbol{J}_1\|^2-\|\boldsymbol{J}_2\|^2)/4I_1^2}, \tag{2.18}$$

implying that $\|\boldsymbol{J}_1\|=$const., $\|\boldsymbol{J}_2\|=$const., $\boldsymbol{J}_1\perp\boldsymbol{J}_2$, *and* $\boldsymbol{J}_2$ *traces a periodic trajectory on the sphere which is a great circle, with natural frequency given as*

$$\omega = \frac{I_1^2\|\boldsymbol{J}_1\|}{\pi(4I_1^2+(\|\boldsymbol{J}_1\|^2-\|\boldsymbol{J}_2\|^2))}. \tag{2.19}$$

(*ii*) *For* $N=1$ *and* $\Omega\neq0$, *one obtains*

$$\dot{\boldsymbol{J}}_1 = \Omega\hat{\boldsymbol{e}}_z\times\boldsymbol{J}_1, \tag{2.20}$$

$$\dot{\boldsymbol{J}}_2 = \frac{1}{4\pi}\frac{\boldsymbol{J}_1\times\boldsymbol{J}_2}{1+(\|\boldsymbol{J}_1\|^2-\|\boldsymbol{J}_2\|^2)/4I_1^2}+\Omega\hat{\boldsymbol{e}}_z\times\boldsymbol{J}_2, \tag{2.21}$$

implying that $\|\boldsymbol{J}_1\|=$const., $\|\boldsymbol{J}_2\|=$const., $\boldsymbol{J}_1\perp\boldsymbol{J}_2$. $\boldsymbol{J}_1$ *traces out a spherical cap, as shown in figure 1, while* $\boldsymbol{J}_2$*'s trajectory decomposes into a linear superposition of rotations around the North Pole axis with frequency* Ω *and rotations around* $\boldsymbol{J}_1$ *with natural frequency* ω *given by* (*2.19*).

Proof. (i) Taking the dot product of (2.17) with $\boldsymbol{J}_1$ and (2.18) with $\boldsymbol{J}_2$, along with the fact that $\boldsymbol{J}_2\cdot\boldsymbol{J}_1\times\boldsymbol{J}_2=0$, gives $\|\boldsymbol{J}_1\|=$ const. and $\|\boldsymbol{J}_2\|=$ const. By theorem 2.1 we know that $\boldsymbol{J}_1\perp\boldsymbol{J}_2$. Since (2.18) is of the form $\dot{\boldsymbol{J}}_2=\omega(\boldsymbol{J}_1/\|\boldsymbol{J}_1\|)\times\boldsymbol{J}_2$, we know that $\boldsymbol{J}_2$ executes solid-body rotation (see §1 of Newton & Shokraneh 2006) around $\boldsymbol{J}_1$ with frequency given by (2.19). (ii) Taking the dot product of (2.20) with $\boldsymbol{J}_1$ and (2.21) with $\boldsymbol{J}_2$ yields zero on the r.h.s.s which implies that $\|\boldsymbol{J}_1\|=$ const. and $\|\boldsymbol{J}_2\|=$ const. Again, theorem 2.1 implies that $\boldsymbol{J}_1\perp\boldsymbol{J}_2$. Equation (2.20) implies that $\boldsymbol{J}_1$ executes solid-body motion with frequency Ω around the North Pole axis, while (2.21) implies that $\boldsymbol{J}_2$ executes a linear combination of solid-body rotations around $\boldsymbol{J}_1$ with frequency ω and the North Pole axis with frequency Ω. ■

3. Charged billiard interactions

For two or more dipoles, the interaction terms cause the centroid path of each to deviate from its underlying geodesic trajectory; hence we view each 'ballistic element' as a *billiard* (see Tabachnikov 1995) and we can think of (2.15) and

(2.16) as a system of 'charged billiard' equations. Although billiard systems have recently been studied on surfaces of constant curvature, such as a sphere (see Gutkin *et al.* 1999), the closest related work seems to be the rather large and growing literature on classical billiard systems in magnetic fields introduced by Robnik & Berry (1985) and studied on surfaces of constant curvature by Gutkin (2001). The integrability and ergodicity of these systems are studied in Berglend & Kunz (1996). In our system, because the nominal distance $\|\boldsymbol{x}_\alpha - \boldsymbol{x}_{\alpha+N}\|$ between each of the point vortices which constitute a given dipole is no longer constant, it is useful to think of each as represented by its centroid coordinate, $\boldsymbol{J}_{\alpha+N}$, and although the centres of vorticity, $\boldsymbol{J}_\alpha$, of each of these billiards is no longer a conserved quantity, their sum over all the billiards is conserved. It is also noted that in the limit when the distance between each pair of point vortices constituting a dipole reaches zero (and their strengths are properly scaled), a point dipole dynamical system can be introduced (see details in Newton 2005) where each point moves along its centroid path.

(*a*) *N*=2*: fundamental interactions*

We start with the most important case of two interacting dipoles, whose equations in the dipole coordinates are given by,

$$\begin{aligned}\dot{\boldsymbol{J}}_1 &= \Omega\hat{e}_z\times\boldsymbol{J}_1\\ &\quad+\frac{\Gamma_1\Gamma_2}{4\pi}\left\{\frac{(\boldsymbol{J}_2+\boldsymbol{J}_4)\times(\boldsymbol{J}_1+\boldsymbol{J}_3)}{4\Gamma_1\Gamma_2-(\boldsymbol{J}_1+\boldsymbol{J}_3)\cdot(\boldsymbol{J}_2+\boldsymbol{J}_4)}-\frac{(\boldsymbol{J}_2-\boldsymbol{J}_4)\times(\boldsymbol{J}_1+\boldsymbol{J}_3)}{4\Gamma_1\Gamma_2+(\boldsymbol{J}_1+\boldsymbol{J}_3)\cdot(\boldsymbol{J}_2-\boldsymbol{J}_4)}\right.\\ &\quad\left.+\frac{(\boldsymbol{J}_2+\boldsymbol{J}_4)\times(\boldsymbol{J}_1-\boldsymbol{J}_3)}{4\Gamma_1\Gamma_2+(\boldsymbol{J}_1-\boldsymbol{J}_3)\cdot(\boldsymbol{J}_2+\boldsymbol{J}_4)}+\frac{(\boldsymbol{J}_2-\boldsymbol{J}_4)\times(\boldsymbol{J}_1-\boldsymbol{J}_3)}{4\Gamma_1\Gamma_2-(\boldsymbol{J}_1-\boldsymbol{J}_3)\cdot(\boldsymbol{J}_2-\boldsymbol{J}_4)}\right\},\end{aligned}\tag{3.1}$$

$$\begin{aligned}\dot{\boldsymbol{J}}_3 &= \frac{1}{4\pi}\frac{\boldsymbol{J}_1\times\boldsymbol{J}_3}{1+\frac{1}{4\Gamma_1^2}(\|\boldsymbol{J}_1\|^2-\|\boldsymbol{J}_3\|^2)}+\Omega\hat{e}_z\times\boldsymbol{J}_3\\ &\quad+\frac{\Gamma_1\Gamma_2}{4\pi}\left\{\frac{(\boldsymbol{J}_2+\boldsymbol{J}_4)\times(\boldsymbol{J}_1+\boldsymbol{J}_3)}{4\Gamma_1\Gamma_2-(\boldsymbol{J}_1+\boldsymbol{J}_3)\cdot(\boldsymbol{J}_2+\boldsymbol{J}_4)}-\frac{(\boldsymbol{J}_2-\boldsymbol{J}_4)\times(\boldsymbol{J}_1+\boldsymbol{J}_3)}{4\Gamma_1\Gamma_2+(\boldsymbol{J}_1+\boldsymbol{J}_3)\cdot(\boldsymbol{J}_2-\boldsymbol{J}_4)}\right.\\ &\quad\left.-\frac{(\boldsymbol{J}_2+\boldsymbol{J}_4)\times(\boldsymbol{J}_1-\boldsymbol{J}_3)}{4\Gamma_1\Gamma_2+(\boldsymbol{J}_1-\boldsymbol{J}_3)\cdot(\boldsymbol{J}_2+\boldsymbol{J}_4)}-\frac{(\boldsymbol{J}_2-\boldsymbol{J}_4)\times(\boldsymbol{J}_1-\boldsymbol{J}_3)}{4\Gamma_1\Gamma_2-(\boldsymbol{J}_1-\boldsymbol{J}_3)\cdot(\boldsymbol{J}_2-\boldsymbol{J}_4)}\right\},\end{aligned}\tag{3.2}$$

$$\begin{aligned}\dot{\boldsymbol{J}}_2 &= \Omega\hat{e}_z\times\boldsymbol{J}_2\\ &\quad+\frac{\Gamma_1\Gamma_2}{4\pi}\left\{\frac{(\boldsymbol{J}_1+\boldsymbol{J}_3)\times(\boldsymbol{J}_2+\boldsymbol{J}_4)}{4\Gamma_1\Gamma_2-(\boldsymbol{J}_2+\boldsymbol{J}_4)\cdot(\boldsymbol{J}_1+\boldsymbol{J}_3)}-\frac{(\boldsymbol{J}_1-\boldsymbol{J}_3)\times(\boldsymbol{J}_2+\boldsymbol{J}_4)}{4\Gamma_1\Gamma_2+(\boldsymbol{J}_2+\boldsymbol{J}_4)\cdot(\boldsymbol{J}_1-\boldsymbol{J}_3)}\right.\\ &\quad\left.+\frac{(\boldsymbol{J}_1+\boldsymbol{J}_3)\times(\boldsymbol{J}_2-\boldsymbol{J}_4)}{4\Gamma_1\Gamma_2+(\boldsymbol{J}_2-\boldsymbol{J}_4)\cdot(\boldsymbol{J}_1+\boldsymbol{J}_3)}+\frac{(\boldsymbol{J}_1-\boldsymbol{J}_3)\times(\boldsymbol{J}_2-\boldsymbol{J}_4)}{4\Gamma_1\Gamma_2-(\boldsymbol{J}_2-\boldsymbol{J}_4)\cdot(\boldsymbol{J}_1-\boldsymbol{J}_3)}\right\},\end{aligned}\tag{3.3}$$

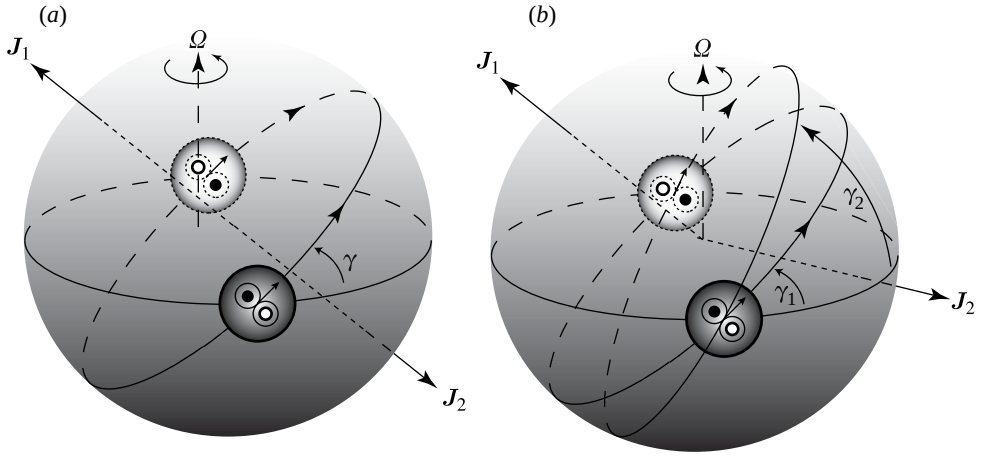

Figure 2. Schematic depicting the interaction parameters between two dipoles. (*a*) Symmetric configuration in which the centre-of-vorticity vectors are aligned and γ denotes the orientation with respect to the equator. (*b*) Generic configuration where the centres of vorticity are not aligned, which requires two angles (γ_1, γ_2) to specify the orientation.

$$\dot{\boldsymbol{J}}_4 = \frac{1}{4\pi}\frac{\boldsymbol{J}_2\times\boldsymbol{J}_4}{1+\frac{1}{4\Gamma_2^2}(\|\boldsymbol{J}_2\|^2-\|\boldsymbol{J}_4\|^2)} + \Omega\hat{e}_z\times\boldsymbol{J}_4$$
$$+\frac{\Gamma_1\Gamma_2}{4\pi}\left\{\frac{(\boldsymbol{J}_1+\boldsymbol{J}_3)\times(\boldsymbol{J}_2+\boldsymbol{J}_4)}{4\Gamma_1\Gamma_2-(\boldsymbol{J}_2+\boldsymbol{J}_4)\cdot(\boldsymbol{J}_1+\boldsymbol{J}_3)} - \frac{(\boldsymbol{J}_1-\boldsymbol{J}_3)\times(\boldsymbol{J}_2+\boldsymbol{J}_4)}{4\Gamma_1\Gamma_2+(\boldsymbol{J}_2+\boldsymbol{J}_4)\cdot(\boldsymbol{J}_1-\boldsymbol{J}_3)}\right.$$
$$\left.-\frac{(\boldsymbol{J}_1+\boldsymbol{J}_3)\times(\boldsymbol{J}_2-\boldsymbol{J}_4)}{4\Gamma_1\Gamma_2+(\boldsymbol{J}_2-\boldsymbol{J}_4)\cdot(\boldsymbol{J}_1+\boldsymbol{J}_3)} - \frac{(\boldsymbol{J}_1-\boldsymbol{J}_3)\times(\boldsymbol{J}_2-\boldsymbol{J}_4)}{4\Gamma_1\Gamma_2-(\boldsymbol{J}_2-\boldsymbol{J}_4)\cdot(\boldsymbol{J}_1-\boldsymbol{J}_3)}\right\}. \quad (3.4)$$

The centres of vorticity are represented by the coordinates $(\boldsymbol{J}_1, \boldsymbol{J}_2)$, while the centroid of each is given by $(\boldsymbol{J}_3, \boldsymbol{J}_4)$. We use these coordinates to integrate the system using a seventh/eighth-order variable time step Runga–Kutta method which is quite accurate for the time scales we consider and throughout the scattering phase. Our initial set-up is depicted in figure 2, where we show the two dipoles at opposite sides of the sphere with their centroids initially located at antipodal points along the equator. A special symmetric case is depicted in figure 2*a* where the dipoles are headed directly towards each other. In this case, their centre-of-vorticity vectors ($\boldsymbol{J}_1$ and $\boldsymbol{J}_2$) are aligned and the orientation of the system with respect to the equator is denoted by the angle γ. The more generic case is shown in figure 2*b* where the centre-of-vorticity vectors are not perfectly aligned, hence one requires two angles (γ_1, γ_2) to fully specify the initial configuration.

(*b*) *Exchange scattering*

The first and the simplest example of a scattering event is called exchange scattering and is shown in figures 3 (non-rotating) and 4 (rotating). A symmetric case of exchange scattering of two equal strength dipoles that initially have orientation $\gamma_1=\gamma_2=\pi/2$ is shown. In this case $\boldsymbol{J}_1+\boldsymbol{J}_2\equiv\boldsymbol{J}=0$.

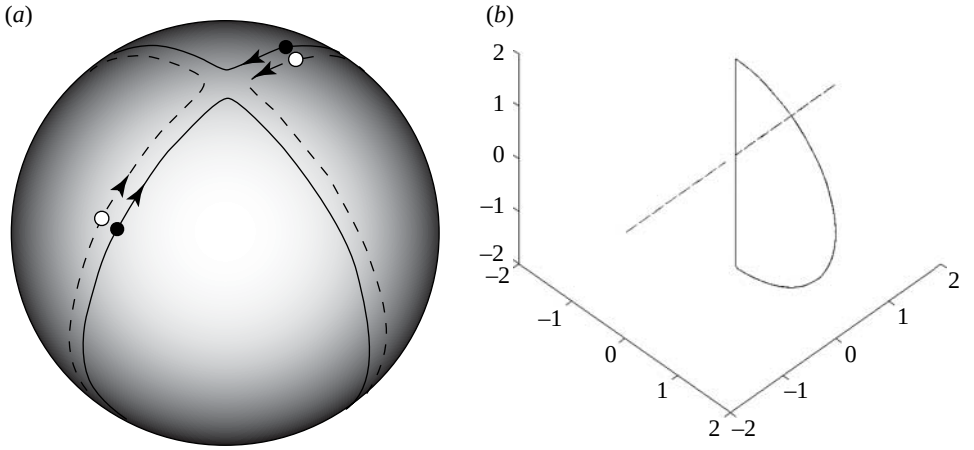

Figure 3. Symmetric exchange scattering on non-rotating sphere for $\boldsymbol{J}=0$ equal dipoles. (*a*) Head on exchange taking place at the North and South Poles, alternating periodically. (*b*) Dipole coordinates of the event. The straight (dashed) curves represent the centre-of-vorticity variable, while the solid curve represents the centroids.

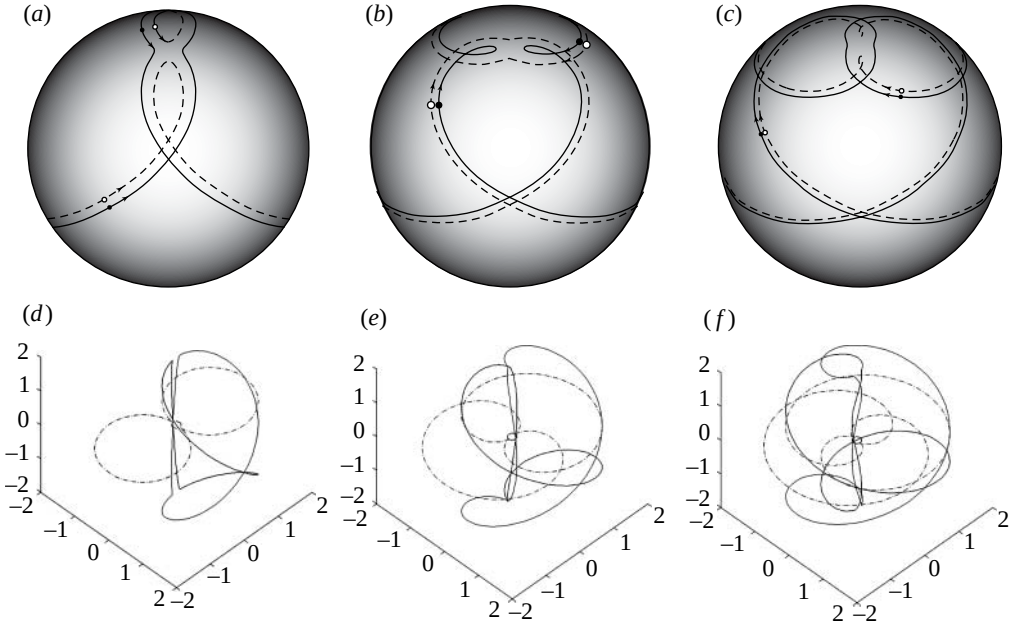

Figure 4. Symmetric exchange scattering on rotating sphere for $\boldsymbol{J}=0$ equal dipoles. With these initial conditions, two exchange events take place at antipodal points during one periodic cycle. (*a*) $\omega:\Omega=1:1$ frequency ratio, (*b*) $\omega:\Omega=2:1$ frequency ratio, (*c*) $\omega:\Omega=3:1$ frequency ratio, (*d*) dipole coordinates for (*a*). The dashed curves represent the centre-of-vorticity variable, while the solid curves represent the centroids; (*e*) dipole coordinates for (*b*) and (*f*) dipole coordinates for (*c*).

Two exchange events take place per cycle (i.e. the dipoles exchange partners) at antipodal points on the sphere (when there is no rotation or when the antipodal points lie on the axis of rotation). Figure 3*a* shows the vortex paths on the non-rotating sphere, while figure 3*b* shows the corresponding dipole coordinates

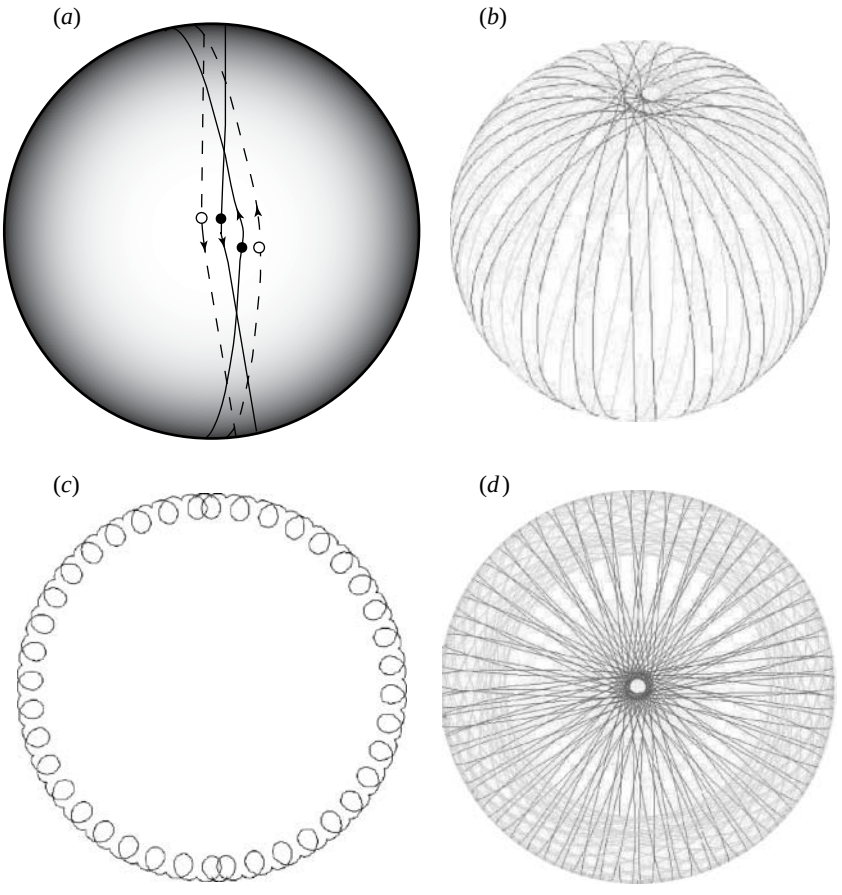

Figure 5. Non-exchange-scattering event between two equal strength dipoles. Each dipole retains its partner throughout the event. (*a*) Non-rotating sphere ($\gamma_1=90°$, $\gamma_2=80°$), (*b*) long-time trajectory (actual vortex paths) on the rotating sphere, (*c*) rotating sphere with $\omega:\Omega=1:1$ frequency ratio ($\gamma_1=90°$, $\gamma_2=0°$). Tips of the centre-of-vorticity vectors, and (*d*) same as (*c*) but shown are the tips of the centroid vectors.

associated with the event. We note that the vortex trajectories in this case are the same as those that would result from vortex motion in a wedge domain on the sphere where each vortex is paired with its image vortex, as discussed in Kidambi & Newton (2000) and Crowdy (2006). Figure 4*a* shows the exchange scattering on the rotating sphere with a $\omega:\Omega=1:1$ frequency ratio, while figure 4*b*,*c* shows the same event on the rotating sphere where the ratio of dipole frequencies to rotation frequencies are (*b*) $\omega:\Omega=2:1$; (*c*) $\omega:\Omega=3:1$. Figure 4*d*–*f* shows the same events but in the dipole coordinate system. The centroid paths are solid.

(*c*) *Non-exchange scattering*

The second scattering event, called *non-exchange* scattering is depicted in figure 5 for two equal strength dipoles that retain their partners throughout the cycle. Figure 5*a* shows the basic interaction on the non-rotating sphere in the

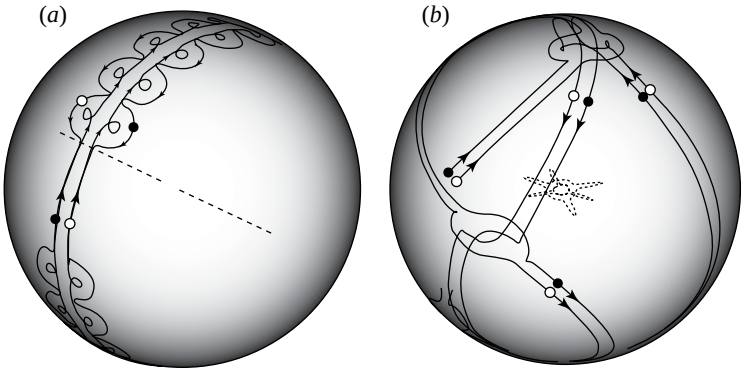

Figure 6. Loop exchange scattering (head on) events for unequal dipoles. The vortex trajectories are depicted as solid curves while the centres of vorticity are depicted as dashed curves. (*a*) Non-rotating and (*b*) rotating sphere with $\omega_1 : \Omega = 1 : 1$ frequency ratio.

case where $\boldsymbol{J} \neq 0$. Although there is a clear interaction between the two dipoles as indicated by the deviation of the dipoles from great circle paths, no partner exchange takes place throughout the period and the dipoles avoid direct collision. Figure 5*b* shows a long-time trajectory on the rotating sphere, while figure 5*c* shows the tips of the centre-of-vorticity vectors during this event. Whether the orbit shown in figure 5*b* ultimately closes up, or densely covers a portion of the spherical surface crucially depends on the initial orientation of the two dipoles, and both periodic orbits and quasi-periodic orbits coexist. Figure 5*d* shows the centroid vectors for the rotating sphere where the frequency ratio is $\omega : \Omega = 1 : 1$.

(*d*) *Loop scattering*

Shown in figure 6 is an example of a loop-scattering interaction (head on) for two unequal dipoles in which the frequency ratio is $\omega_1 : \omega_2 = 3 : 1$. Figure 6*a* shows a case with dipole strengths $\Gamma_1 = -\Gamma_3 = 1.0$ and $\Gamma_2 = -\Gamma_4 = 3.0$ with orientations $\gamma_1 = \gamma_2 = \pi/2$ on the non-rotating sphere. The dipoles perform a sequence of loops as they travel around the sphere; the number of loops depends on the frequency ratio of the two dipoles. On each loop, one dipole loops inside the other, which accommodates the passage by splitting around the inner loop. Within the loop, the dipoles exchange partners, forming two new dipoles comprising vortices of opposite sign but unequal magnitude. As a result, they move along curved trajectories within the loop. Figure 6*b* shows the same interaction on the rotating sphere. Shown is a case with unequal dipoles with frequency ratio $\omega_1 : \omega_2 = 2 : 1$ and $\omega_1 : \Omega = 1 : 1$. While the dipole trajectories are relatively complex, the tips of the centre-of-vorticity vectors, shown as dashed curves, move on closed periodic orbits. In this case, the overall trajectory is periodic as these vectors execute closed loops. Figure 7 shows an example of a loop-scattering interaction (head on) with a $\omega_1 : \Omega = 1 : 1$ frequency ratio. We show the vortex trajectories (figure 7*a*), the centre-of-vorticity trajectories (figure 7*b*) and the centroid trajectories (figure 7*c*) projected onto a plane.

By contrast, a loop-scattering interaction that we call a 'chasing' mode is shown in figures 8 and 9. Figure 8*a* shows two unequal dipoles initially aligned so that one chases the other around the non-rotating sphere creating a smaller loop

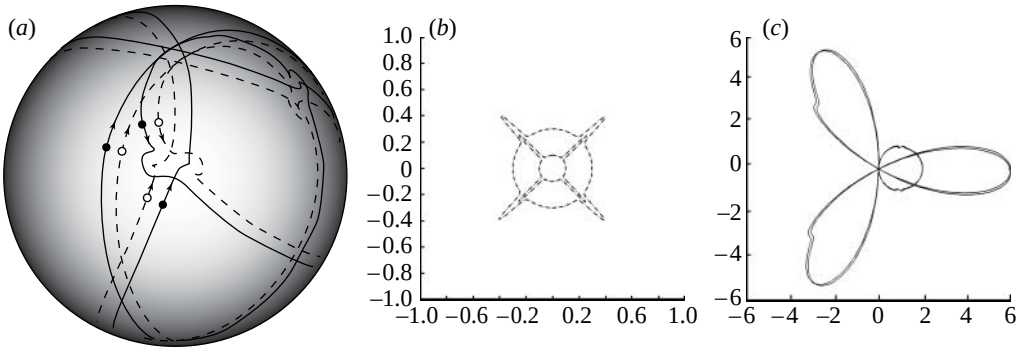

Figure 7. Loop exchange-scattering (head on) events for unequal dipoles on rotating sphere: $\omega_1 : \Omega = 1 : 1$ frequency ratio. (*a*) Vortex trajectories, (*b*) centre-of-vorticity coordinates, and (*c*) centroid coordinates.

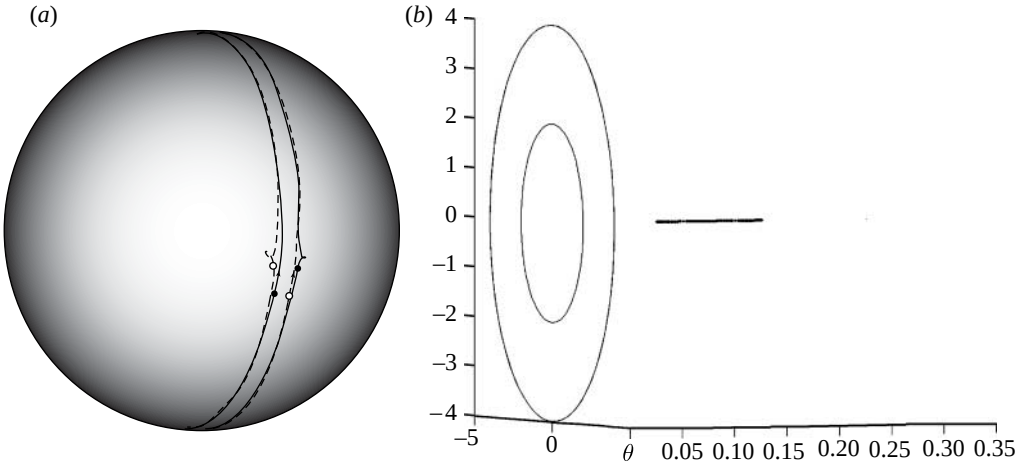

Figure 8. Loop exchange-scattering (chasing) events for unequal dipoles on a non-rotating sphere. (*a*) Vortex trajectories and (*b*) dipole coordinates. The dashed curves represent the centre-of-vorticity variable, while the solid curves represent the centroids.

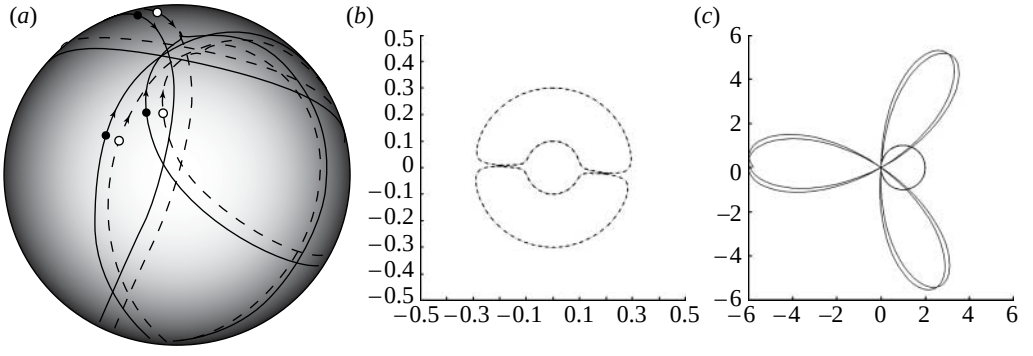

Figure 9. Loop exchange-scattering (chasing) events for unequal dipoles on rotating sphere: $\omega_1 : \Omega = 1 : 1$ frequency ratio. (*a*) Vortex trajectories, (*b*) centre-of-vorticity coordinates, and (*c*) centroid coordinates.

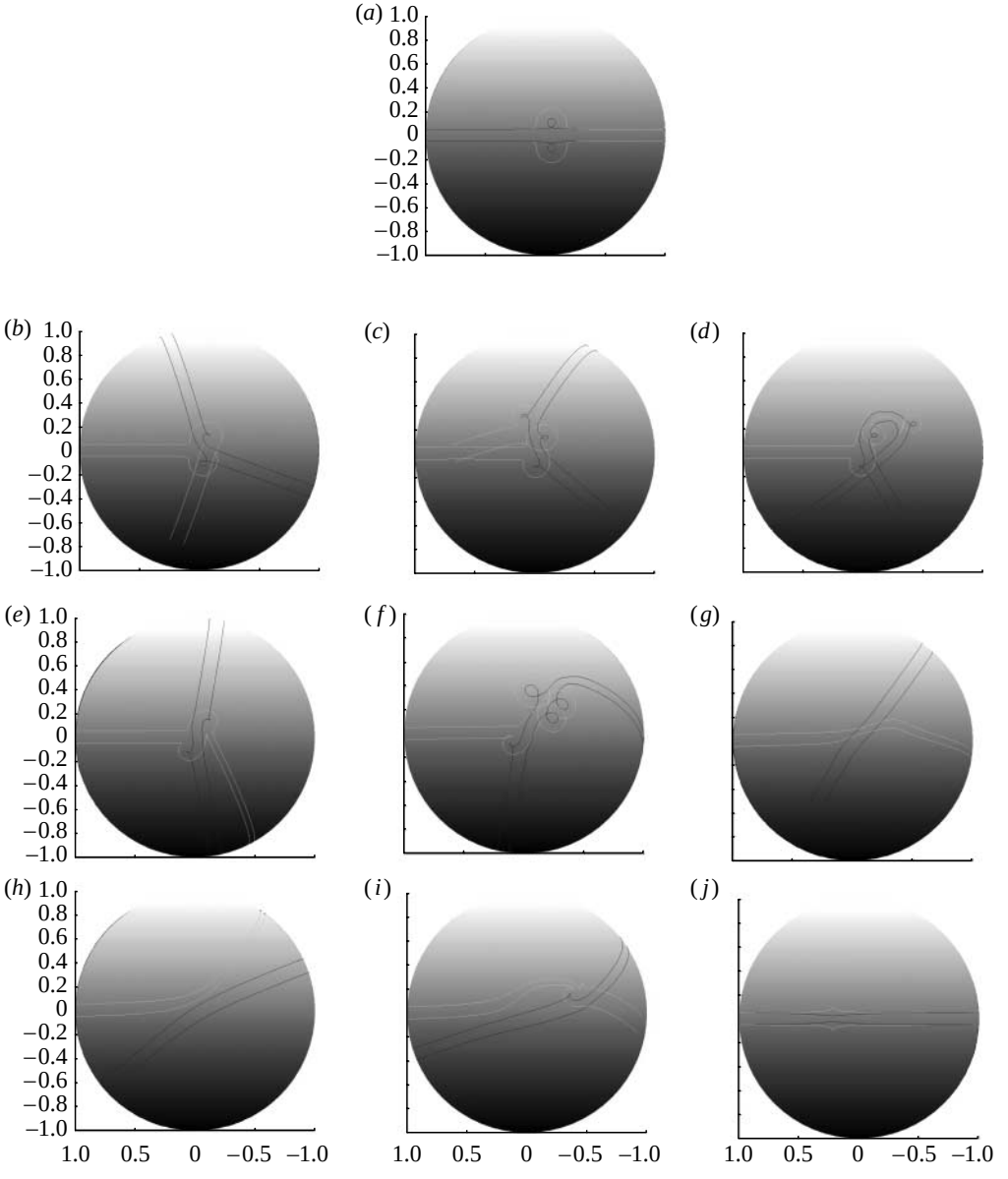

Figure 10. Scattering of two dipoles (unequal) as a function of interaction angle on a non-rotating sphere. Both loop-scattering and non-exchange-scattering events are seen in these sequences. (*a*) $\theta=0°$, (*b*) $\theta=20°$, (*c*) $\theta=40°$, (*d*) $\theta=60°$, (*e*) $\theta=80°$, (*f*) $\theta=100°$, (*g*) $\theta=120°$, (*h*) $\theta=140°$, (*i*) $\theta=160°$, and (*j*) $\theta=180°$.

during the interaction process than the head-on collision. Figure 8*b* shows the dipole coordinates during the interaction. The same interaction on the rotating sphere is shown in the sequence of figure 9*a–c*, with a $\omega_1 : \Omega = 1 : 1$ frequency ratio. This interaction is analogous to the famous 'leapfrogging' behaviour whose analysis in planar systems dates back to the classical work of Love (1894).

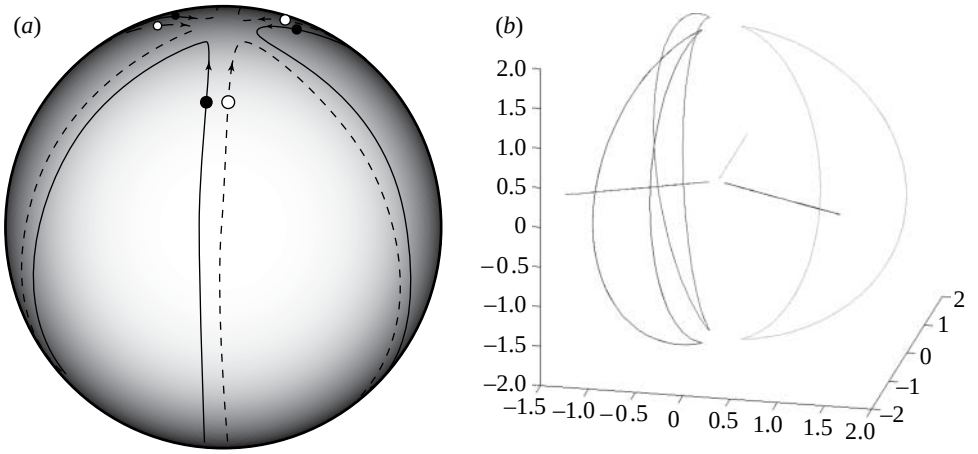

Figure 11. Pure exchange scattering of three equal strength dipoles on a non-rotating sphere: (*a*) vortex trajectories on the sphere and (*b*) dipole coordinates. The dashed curves represent the centre-of-vorticity variable, while the solid curves represent the centroids.

The full gamut of interactions is shown in figure 10 where we depict the scattering of two dipoles as a function of the interaction angle, varying this angle in increments of 20°. From this, we can see that we can have loop-scattering interactions, non-exchange scattering or exchange scattering depending on the angle at which the dipoles are initially oriented.

4. Three dipoles

When three or more dipoles interact, the scattering modes described earlier for the two-dipole system remain central. This is because, unless the initial conditions are chosen judiciously, only two of the dipoles within the system will typically undergo a close interaction at any given time, thus the others affect the interaction only through the far-field. As in the two-dipole case, a pure exchange-scattering event can take place, as shown in figure 11*a*,*b* on the non-rotating sphere. The three equal strength dipoles are aligned initially so that they head for the North Pole. Note that the members of each dipole pair split off near the North Pole and pair up with a member of another dipole as they head for the South Pole. The dipole coordinates are shown in figure 11*b*. Again, the analogy with vortex motion in wedge domains on the sphere as discussed in Kidambi & Newton (2000) and Crowdy (2006) should be clear. Figure 12*a*,*b* shows an interaction of three dipoles on a non-rotating sphere that involves both an exchange event and a loop-scattering event. In figure 13, we show a sphere with all of the previously documented interactions between two dipoles retained for the three-dipole problem in a setting that combines them throughout a more complex evolution. However, if all three approach each other so that they interact simultaneously, as shown in figure 14, a much more complex process occurs that cannot easily be interpreted as combinations of simpler interactions. In a long evolutionary process of multiple dipoles, these types of interactions will not be nearly as common as the simpler interactions between pairs.

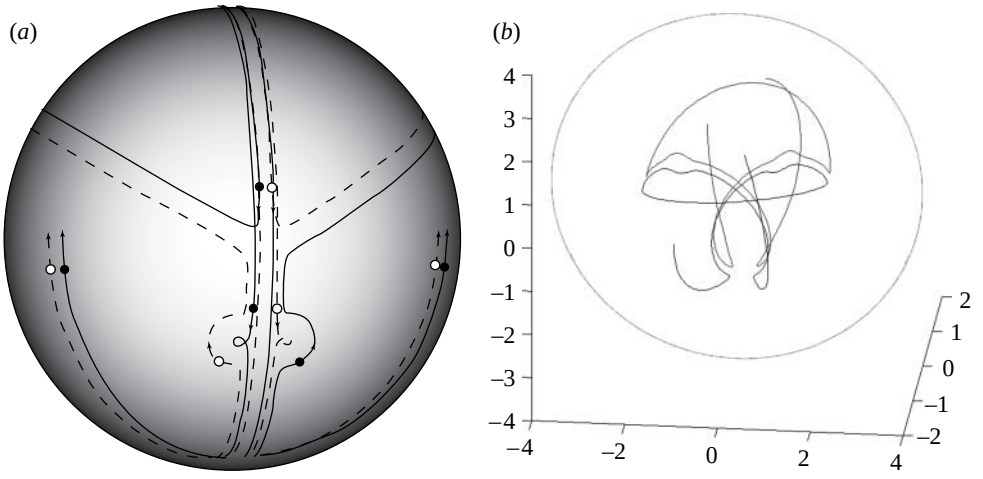

Figure 12. Interaction process of three dipoles, which includes both an exchange-scattering and a loop-scattering interaction on a non-rotating sphere: (*a*) vortex trajectories on the sphere and (*b*) dipole coordinates. The dashed curves represent the centre-of-vorticity variable, while the solid curves represent the centroids.

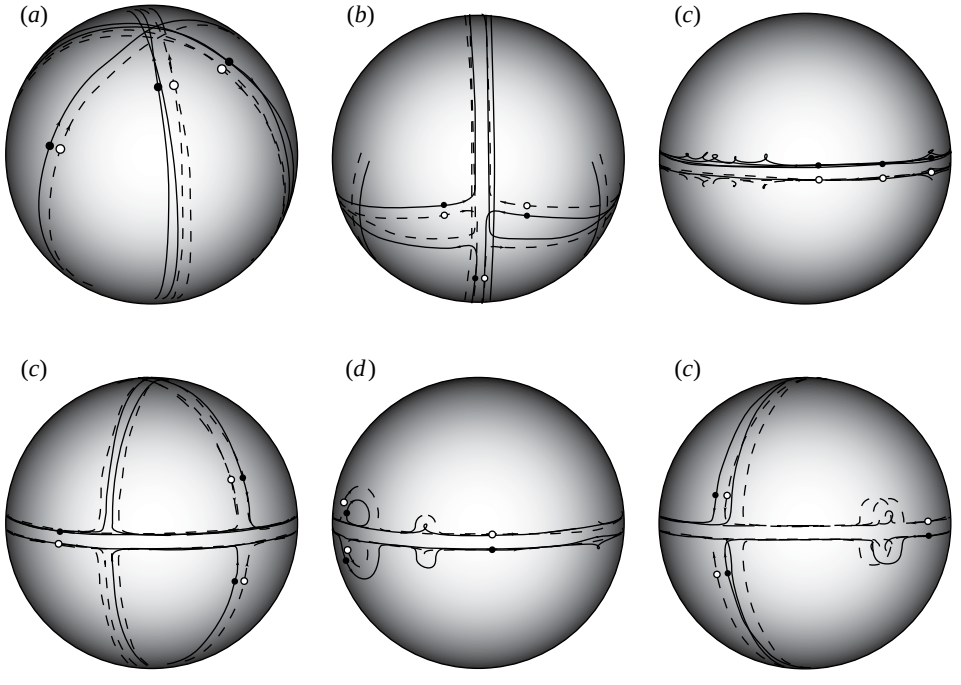

Figure 13. Three-dipole interaction on a sphere (non-rotating) which shows that the basic two dipole interactions are retained, although in a setting that combines them throughout the evolution. (*a*) Non-exchange scattering, (*b*) exchange scattering, (*c*) loop chasing, (*d*) exchange scattering, (*e*) loop scattering, and (*f*) exchange and loop scattering.

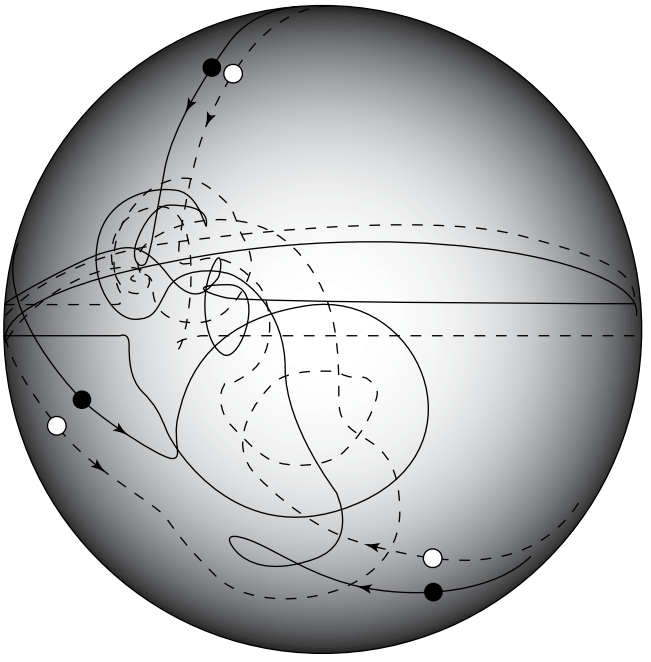

Figure 14. Interaction process of the three dipoles which includes aspects of the two dipole interaction problem but is generally more complex. Shown are the point vortex paths on the sphere.

5. Discussion

The interacting dipole equations (2.15) and (2.16) makes explicit the correspondence between the motion of multiple dipoles and the billiard problem and can be viewed as a system of interacting 'charged' billiards where the dipole strength plays the role of the charge. Previous works, such as that of Kimura (1999), brought to light the fact that the centroid of an isolated dipole on a surface of constant curvature follows a geodesic path, as does a billiard on such a surface (Gutkin *et al.* 1999). However, when multiple dipoles are present, the far-field interactions play a central role in the governing dynamics and cause the trajectories to deviate from great circle paths. Nonetheless, in these coordinates, the equations for the interactions can be viewed as geodesic motion, modified by the complex interaction terms due to the other dipoles. Typically, in a multi-dipole population, only two will come into close contact at a time, hence a key to understanding general interactions is to understand these most basic interactions that we have focused on in this work.

We thank the National Science Foundation for support under the grant NSF-DMS-0504308.

References

Berglend, N. & Kunz, H. 1996 Integrability and ergodicity of classical billiards in a magnetic field. *J. Stat. Phys.* **83**, 81–126. (doi:10.1007/BF02183641)

Chavanis, P.-H. 2007 Kinetic theory of two-dimensional point vortices from a BBGKY-like hierarchy. *Physica A*. (doi:10.1016/j.physa.2007.09.052)

Chavanis, P. H. & Lemou, M. 2007 Kinetic theory of point vortices in two dimensions: analytical results and numerical simulations. (http://arxiv.org/abs/cond-mat/0703023v1)

Crowdy, D. 2006 Point vortex motion on the surface of a sphere with impenetrable boundaries. *Phys. Fluids* **18**, 036602. (doi:10.1063/1.2183627)

DiBattista, M. T. & Polvani, L. M. 1998 Barotropic vortex pairs on a rotating sphere. *J. Fluid Mech.* **358**, 107–133. (doi:10.1017/S0022112097008100)

Dritschel, D. G. & Zabusky, N. 1996 On the nature of vortex interactions and models in unforced nearly inviscid two-dimensional turbulence. *Phys. Fluids* **8**, 1252–1256. (doi:10.1063/1.868896)

Eckhardt, B. & Aref, H. 1988 Integrable and chaotic motion of four vortices II. Collision dynamics of vortex pairs. *Phil. Trans. R. Soc. A* **326**, 655–696. (doi:10.1098/rsta.1988.0117)

Gutkin, B. 2001 Hyperbolic magnetic billiards on surfaces of constant curvature. *Commun. Math. Phys.* **217**, 33–53. (doi:10.1007/s002200000346)

Gutkin, B., Smilansky, U. & Gutkin, E. 1999 Hyperbolic billiards on surfaces of constant curvature. *Commun. Math. Phys.* **208**, 65–90. (doi:10.1007/s002200050748)

Jamaloodeen, M. I. & Newton, P. K. 2006 The *N*-vortex problem on a rotating sphere: II. Heterogeneous platonic solid equilibria. *Proc. R. Soc. A* **462**, 3277–3299. (doi:10.1098/rspa.2006.1731)

Kidambi, R. & Newton, P. K. 1998 Motion of three point vortices on a sphere. *Physica D* **116**, 143–175. (doi:10.1016/S0167-2789(97)00236-4)

Kidambi, R. & Newton, P. K. 2000 Point vortex motion on a sphere with solid boundaries. *Phys. Fluids* **12**, 581–588. (doi:10.1063/1.870263)

Kimura, Y. 1999 Vortex motion on surfaces of constant curvature. *Proc. R. Soc. A* **455**, 245–259. (doi:10.1098/rspa.1999.0311)

Love, A. E. H. 1894 On the motion of paired vortices with a common axis. *Proc. Lond. Math. Soc.* **25**, 185–194. (doi:10.1112/plms/s1-25.1.185)

Marmanis, H. 1998 The kinetic theory of point vortices. *Proc. R. Soc. A* **454**, 587–606. (doi:10.1098/rspa.1998.0175)

McDonald, N. R. 1999 The motion of geophysical vortices. *Phil. Trans. R. Soc. A* **357**, 3427–3444. (doi:10.1098/rsta.1999.0501)

Newton, P. K. 2001 *The N-vortex problem: analytical techniques. Applied mathematical sciences*, vol. 145. New York, NY: Springer.

Newton, P. K. 2005 The dipole dynamical system. *Disc. Cont. Dyn. Syst. B* (Suppl.), 692–699.

Newton, P. K. & Mezić, I. 2002 Non-equilibrium statistical mechanics for a vortex gas. *J. Turbulence* **3**, 1–7.

Newton, P. K. & Ross, S. D. 2006 Chaotic advection in the restricted four-vortex problem on a sphere. *Physica D* **223**, 36–53. (doi:10.1016/j.physd.2006.08.012)

Newton, P. K. & Sakajo, T. 2007 The *N*-vortex problem on a rotating sphere: III. Ring configurations coupled to a background field. *Proc. R. Soc. A* **463**, 961–977. (doi:10.1098/rspa.2006.1802)

Newton, P. K. & Shokraneh, H. 2006 The *N*-vortex problem on a rotating sphere: I. Multi-frequency configurations. *Proc. R. Soc. A* **462**, 149–169. (doi:10.1098/rspa.2005.1566)

Robnik, M. & Berry, M. V. 1985 Classical billiards in magnetic fields. *J. Phys. A: Math. Gen.* **18**, 1361–1378. (doi:10.1088/0305-4470/18/9/019)

Tabachnikov, S. 1995 *Billiards. Panor, syntheses*, vol. 1. Paris, France: Société Mathématique de France.